Tailoring the air plasma with a double laser pulse

M. N. Shneider,[1] A. M. Zheltikov,[2,3] and R. B. Miles[1]
[1]*Department of Mechanical and Aerospace Engineering, Princeton University, Princeton, New Jersey 08544-5263, USA*
[2]*Physics Department, International Laser Center, M. V. Lomonosov Moscow State University, Moscow 119992, Russia*
[3]*Department of Physics and Astronomy, Texas A&M University, College Station, Texas 77843-4242, USA*

(Received 14 March 2011; accepted 26 May 2011; published online 28 June 2011)

We present a comprehensive model of plasma dynamics that enables a detailed understanding of the ways the air plasma induced in the atmosphere in the wake of a laser-induced filament can be controlled by an additional laser pulse. Our model self-consistently integrates plasma-kinetic, Navier–Stokes, electron heat conduction, and electron–vibration energy transfer equations, serving to reveal laser–plasma interaction regimes where the plasma lifetime can be substantially increased through an efficient control over plasma temperature, as well as suppression of attachment and recombination processes. The model is used to quantify the limitations on the length of uniform laser-filament heating due to the self-defocusing of laser radiation by the radial profile of electron density. The envisaged applications include sustaining plasma guides for long-distance transmission of microwaves, standoff detection of impurities and potentially hazardous agents, as well as lightning control and protection. © *2011 American Institute of Physics*. [doi:10.1063/1.3601764]

INTRODUCTION

Remote control of plasmas induced by laser radiation in the atmosphere is one of the challenging issues of free-space communication, long-distance energy transmission, remote sensing of the atmosphere, and standoff detection of trace gases and biothreat species. Sequences of laser pulses, as demonstrated by an extensive earlier work (see, e.g., Refs. 1–3), offer an advantageous tool providing access to the control of air-plasma dynamics and optical interactions. Recently, Henis *et al.*[4] have proposed to use a dual femtosecond/nanosecond laser pulse to enhance the energy density locally deposited in a laser-induced plasma in the atmosphere. Recent experiments by Zhou *et al.*[5] have demonstrated that the lifetime of plasma channels generated through filamentation of femtosecond laser pulses can be increased by applying a delayed nanosecond pulse. A similar scenario has been observed[6] in the regime of resonance enhanced multiphoton ionization (REMPI), involving an avalanche hybrid ionization of a gas by nanosecond laser pulses with intensities well below the breakdown threshold. Close enough to these problems is the evolution of the plasma channel created in the atmospheric air by a femtosecond pre-ionizing laser pulse with an external DC electric field studied in Refs. 7 and 8.

Several important applications of air-plasma tailoring with a double laser pulse are envisaged. First, this approach can improve the detection sensitivity of the radar—REMPI diagnostic technique add[9] strongly promoting its application for standoff detection.[10] Second, the double-pulse method can help to generate laser plasmas at reduced gas densities, e.g., at high altitudes in aerospace applications. Third, using an additional heating laser pulse may be instrumental in resolving the issues of laser ignition,[11,12] with the first pulse providing pre-ionization in a gas chamber, thus substantially reducing the requirements for the main, combustion-igniting laser or microwave pulse. In a prototype experiment implemented recently at Princeton,[13] a femtosecond laser pulse was employed to pre-ionize a gas, with additional gas heating provided by a subsequent microsecond microwave pulse, whose intensity was well below the breakdown threshold. Fourth, ionization of the atmosphere using double laser pulses suggests interesting options for the manipulation and long-distance transmission of microwaves.[14–16] Arrays of laser-induced filaments have been shown to form waveguides for microwaves[15,16] enabling, in particular, a guided-wave delivery of radar radiation for long-distance communication and stand-off detection of biothreat species in the atmosphere. In a recent experiment, Châteauneuf *et al.*[17] have employed a 100-TW femtosecond laser source to generate a cylindrical array of more than 1000 filaments, forming a waveguide for 10-GHz radiation. Organic impurities and pollutions, e.g., those found in abundance in the summertime smog of big cities, have been shown[18] to facilitate the creation of plasma guides for microwave radiation. Common to all these methods is the problem of fast plasma decay in the wake of the femtosecond laser pulse, which leads to dramatic limitations on the lifetime of plasma-based waveguides.

In this work, we present a model that allows a detailed quantitative analysis of plasma dynamics induced by additional laser pulses used to tailor the properties of plasmas decaying in the wake of a laser filament in the atmosphere. We show that, with an appropriate optimization of parameters of plasma-tailoring laser pulses, an uncontrolled gas breakdown due to avalanche ionization can be avoided. The model of atmospheric plasma decay used in the analysis presented below in this paper modifies the model developed

in our earlier work[16] toward a more realistic description of excitation, relaxation, and recombination processes in the multicomponent plasma of atmospheric air. This model is applied below to identify the ways the air plasma induced in the atmosphere in the wake of a laser-induced filament can be controlled by an additional laser pulse.

IONIZATION IN A FILAMENT INDUCED BY A FEMTOSECOND LASER PULSE

We consider a filament induced by Ti: sapphire femtosecond laser pulses with a central wavelength $\lambda_1 = 800$ nm. For a rectangular laser pulse of duration τ_1, the electron density is estimated as

$$n_e = n_{O_2^+} + n_{N_2^+} \approx [N_{O_2}\varpi_{O_2} + N_{N_2}\varpi_{N_2}]\tau_1, \quad (1)$$

where n_e is the electron density, $n_{O_2^+}$ and $n_{N_2^+}$ are the densities of oxygen and nitrogen molecular ions, respectively, N_{O_2} and N_{N_2} are the densities of oxygen and nitrogen molecules, and $\varpi_{O_2}, \varpi_{N_2}$ are the photoionization rates of oxygen and nitrogen molecules. The rates $\varpi_{O_2}, \varpi_{N_2}$ were calculated (see, e.g., Ref. 19) on the basis of a modified Keldysh theory.[20] For laser pulses with an intensity $I_{fs} = 4 \times 10^{13}$ W/cm^2 and pulse width $\tau_1 = 100$ fs, we find $n_{O_2^+} = 1.02 \times 10^{23}$m^{-3}, $n_{N_2^+} = 4.08 \times 10^{20}$m^{-3}, and $n_e = 1.024 \times 10^{23}$m^{-3}.

To mimic typical plasma parameters in a filament induced in air by a femtosecond laser pulse,[21–23] we take the following initial conditions for the plasma parameters at the instant of time $t = 0$: $T_e = 1$ eV, $T = T_v = 300$ K, and

$$n_e = (n_{O_2^+} + n_{N_2^+}) \approx 1 \cdot 10^{23} \exp(-r/r_b^2), \quad (2)$$

with $r_b = 50$ μm. These results for the electron and ion densities are used as initial conditions in simulations of the decaying air plasma.

FILAMENT PLASMA DECAYING AND A SECOND LASER PULSE

With an assumption of a cylindrical geometry of plasma decay, the continuity equations for all plasma species are written as

$$\frac{\partial [n_s]}{\partial t} + \frac{1}{r}\frac{\partial (r[\Gamma_s])}{\partial r} = [G_s] - [L_s], \quad (3)$$

where n_s are the densities of N_2^+, O_2^+, N_4^+, O_4^+, NO^+, O^+ (n_+), e(n_e), O_2^-, O^- (n_-), O, N, NO, O_3, and G_s, L_s are the corresponding generation and loss rates. The charge particles fluxes Γ_s appearing in Eq. (3) are defined by the equations

$$\Gamma_{e,-} = -\mu_{e,-} n_{e,-} E - D_{e,-}\frac{\partial n_{e,-}}{\partial r} + n_{e,-} u, \quad (4)$$

for electrons (Γ_e) and O_2^-, O^- ions (Γ_-);

$$\Gamma_{i,+} = \mu_{i,+} n_{i,+} E - D_{i,+}\frac{\partial n_{i,+}}{\partial r} + n_{i,+} u, \quad (5)$$

for the ith sort of positive ions, and

$$\Gamma_n = -D_n \frac{\partial n_n}{\partial r} + n_n u, \quad (6)$$

for neutral species.

Here, $\mu_e = em^{-1}(\nu_m + \nu_c)^{-1}$ is the electron mobility, $\mu_{i,+}$ and μ_- are the mobilities of positive and negative ions, respectively, $D_e = \mu_e T_e$, $D_{i,+} = \mu_{i,+} T$, and $D_- = \mu_- T$ are the relevant diffusion coefficients, T is the translational temperature of the gas in eV, and T_e is the electron temperature in electron volts. The last terms in Eqs. (4)–(6) become important for prebreakdown or breakdown intensities of the plasma-tailoring laser field or long time intervals ($\gg$10 ns); $\nu_m \approx 3.91 \times 10^{-14} N T_e^{1/2}$ is the electron-neutral transport frequency, $\nu_c = 2.91 \times 10^{-12} n_e T_e^{-3/2} \ln\Lambda$ is the electron-ion Coulomb collision frequency,[24,25] N is the air density in m^{-3}, and ln Λ is the Coulomb logarithm. The mobilities for positive and negative ions are given by equal $\mu_{+,-} = 0.21/(p \cdot 300/T)$ (in m^2 V^{-1} s^{-1}), where p is the air pressure in Torr and the temperature T is in K; u is the gas velocity.

The radial field component $E = -\partial\phi/\partial r$ is calculated by solving the Poisson equation for the potential ϕ,

$$\frac{1}{r}\frac{\partial}{\partial r}\left(r\frac{\partial \phi}{\partial r}\right) = -\frac{e}{\varepsilon_0}\left(\sum_i n_{i,+} - \sum_k n_{k,-} - n_e\right), \quad (7)$$

with boundary conditions $\partial\phi/\partial r|_{r=0} = 0$ and $\phi(\infty) = 0$. Summations in Eq. (7) are done over all types of positive and negative ions.

The intensity of the subsequent infrared laser pulse is assumed to be too low to induce any noticeable ionization effects in the surrounding air. However, at elevated intensities, cascade ionization in the pre-ionized filament by electrons oscillating in the laser field becomes significant. While a rigorous calculation of ν_i involves the solution of the relevant quantum kinetic equation, in this work, we choose an empirical relation taken from[26]

$$\nu_i(T_e) = \nu_{i,N_2} + \nu_{i,O_2};$$

$$\nu_{i,N_2} \approx \left(p_{[Torr]}\frac{300}{T_{[K]}}\frac{10^7}{\sqrt{T_e}}\right)\left[\left(14.093 + 27.366T_e + 1.386T_e^2\right) \times \exp\left(-\frac{15.58}{T_e}\right)\right]; \quad (8a)$$

$$\nu_{i,O_2} \approx \left(p_{[Torr]}\frac{300}{T_{[K]}}\frac{10^7}{\sqrt{T_e}}\right)\left[\left(1.43 + 2.47T_e + 0.456T_e^2\right) \times \exp\left(-\frac{12.06}{T_e}\right)\right]. \quad (8b)$$

Note that because of the assumption of a Maxwellian electron distribution function, an application of these formulas to a nonionized or weakly ionized air leads to an overestimation of the ionization rates at electron temperatures $T_e \sim 1$ eV. However, in the case of air plasma with a relatively high electron density induced by a femtosecond laser pulse, we can assume that the electron density distribution is

Maxwellian due to the high rate of electron-electron Coulomb collisions.

Electron photodetachment processes, with a rate

$$\left(\frac{\partial n_e}{\partial t}\right)_{phd} = -\left(\frac{\partial n_-}{\partial t}\right)_{phd} = \sigma_{ph}\left[\frac{I_L(r,t)}{\hbar\omega_L}\right]n_-, \tag{9}$$

contribute to the electron generation and the loss of negative ions, with $I_L(r,t)$ being the intensity of the plasma-tailoring laser field, ω_L being the frequency of this radiation, and σ_{ph} being the cross section of electron photodetachment from O_2^- ions in the atmosphere through the $\hbar\omega_L + O_2^-(^4\Sigma_g^-) \rightarrow e + O_2(^3\Sigma_g^-)$ process.[27] We have neglected the photodetachment from O^- atomic ions, because the threshold for this process ($\approx$1.4 eV (Ref. 27)) exceeds the photon energy $\hbar\omega_L$ for subsequent heating by infrared laser radiation considered in the present work.

Parameters of the gas flow are defined by solving axially symmetric Navier–Stokes equations,

$$\frac{\partial\rho}{\partial t} + \frac{1}{r}\frac{\partial(r\rho u)}{\partial r} = 0, \tag{10}$$

$$\frac{\partial\rho u}{\partial t} + \frac{1}{r}\frac{\partial(r\rho u^2)}{\partial r} = -\frac{\partial p}{\partial r} + \tfrac{2}{3}\eta\left(\frac{1}{r}\frac{\partial}{\partial r}\left(r\left(2\frac{\partial u}{\partial r} - \frac{u}{r}\right)\right) + \frac{1}{r}\frac{\partial u}{\partial r} - \frac{u}{r^2}\right), \tag{11}$$

$$\frac{\partial\rho(\varepsilon + u^2/2)}{\partial t} + \frac{1}{r}\frac{\partial(r[\rho(\varepsilon + u^2/2) + p]u)}{\partial r} = Q + \frac{1}{r}\frac{\partial}{\partial r}\left(r\lambda_h\frac{\partial T}{\partial r}\right) + \tfrac{2}{3}\eta\left[\frac{1}{r}\left(\frac{\partial}{\partial r}\left(ru\left(2\frac{\partial u}{\partial r} - \frac{u}{r}\right)\right)\right)\right]. \tag{12}$$

Here, p and ε are the gas pressure and energy, ρ is the gas density, and λ_h and η are the heat conductivity and viscosity of the gas, and

$$Q \equiv Q(r,t) = Q_{VT} + Q_{eT} + Q_R, \tag{13}$$

where Q_{VT} is the rate of heating due to vibrational-translational (VT) relaxation per unit volume,

$$Q_{eT} = \frac{3}{2}n_e k(T_e - T)\delta(\nu_m + \nu_c) \tag{14}$$

is the rate of direct gas heating due to elastic electron–molecule and Coulomb collisions, k is the Boltzmann constant (T_e and T are in Kelvin). For a weakly ionized air plasma, $\delta \approx 2m(0.2/M_{O_2} + 0.8/M_{N_2}) \approx 2m/M$ and $M \approx M_{N_2}M_{O_2}/(0.8M_{O_2} + 0.2M_{N_2})$, where M_{N_2} is the mass of nitrogen molecules and M_{O_2} is the mass of oxygen molecules; $Q_R \approx \sum_i \varepsilon_{r,i}\beta_{r,i}n_e n_{i,+}$ is the rate of dissociative recombination heating, with the coefficients $\varepsilon_{r,i}$ taking values from the interval 0.04 eV $\leq \varepsilon_r \leq$ 3.4 eV, depending on the sort of molecular ions involved in dissociative recombination[28] (here, we set $\varepsilon_{r,i} = 1$ eV for all the reactions of dissociative recombination), and $\beta_{r,i}$ are the dissociative recombination coefficients (see Table I).

The gas density ρ, pressure p, and energy ε, appearing in the Navier–Stokes equations, are assumed to follow an ideal-gas equation,

$$p = (\gamma - 1)\rho\varepsilon, \tag{15}$$

with $\varepsilon = c_v T$ and $\gamma = c_p/c_v = 1.4$.

Energy transfer to molecular vibrations is included in the model through the equation for the vibrational energy E_v,

$$\frac{\partial E_v}{\partial t} + \frac{1}{r}\frac{\partial(rE_v u)}{\partial r} = Q_{eV} - Q_{VT}, \tag{16}$$

where

$$Q_{eV} = \frac{3}{2}n_e k(T_e - T_v)\nu_{ev}(T_e) \tag{17}$$

is the energy transfer rate of excitation of molecular vibrations due to collisions of molecules with electrons, T_v is the vibrational temperature, and ν_{ev} is the electron–vibration excitation rate.

When the energy E_v is not too far from its equilibrium value E_v^0, we have

$$Q_{VT} = \frac{E_v - E_v^0}{\tau_{VT}}, \tag{18}$$

where

$$E_v = N\varepsilon_v = N\frac{\hbar\omega_0}{\exp(\hbar\omega_0/T_v) - 1}, \tag{19}$$

and

$$E_v^0 = N\varepsilon_v^0 = N\frac{\hbar\omega_0}{\exp(\hbar\omega_0/T) - 1}, \tag{20}$$

where N is the molecular density and ε_v^0 and ε_v are the thermal-equilibrium and nonequilibrium vibrational energies per molecule, respectively,

$$\tau_{VT} = 1/\{N\cdot[7\cdot 10^{-16}\exp(-141/T^{1/3}) + \alpha_O\cdot 5\cdot 10^{-18}\exp(-128/T^{1/2})]\}, \tag{21}$$

τ_{VT} is the VT-relaxation time,[13,16] α_0 is the molar fraction of atomic oxygen, $\hbar\omega_0$ is the vibration quantum ($\hbar\omega_0 = 0.29$ eV for N_2 molecules), and N and T are expressed in m^{-3} in K, respectively.

Electron heat conduction is governed by the equation

$$\frac{\partial}{\partial t}\left(\frac{3}{2}kn_eT_e\right) + \frac{1}{r}\frac{\partial}{\partial r}\left[r\left(\frac{5}{2}\Gamma_e kT_e - \lambda_e\frac{\partial T_e}{\partial r}\right)\right] = J_L - \frac{3}{2}n_e k(T_e - T_v)\nu_{ev} - \frac{3}{2}n_e k(T_e - T)\delta(\nu_m + \nu_c) - n_e(\nu_{i,N_2}I_{N_2} + \nu_{i,O_2}I_{O_2} + \nu_{ex}I^*), \tag{22}$$

where

$$J_L = \frac{e^2 n_e I_L(\nu_m + \nu_c)}{\varepsilon_0 cm[\omega_L^2 + (\nu_m + \nu_c)^2]} \tag{23}$$

TABLE I. List of kinetic processes and rates.

$e + N_2 \rightarrow N_2^+$	Approximation (8a)		Ref. 26
$e + O_2 \rightarrow O_2^+$	Approximation (8b)		Ref. 26
$e + O_2 + O_2 \rightarrow O_2^- + O_2$	$1.4 \times 10^{-41}\left(\frac{300}{T_e}\right)\exp\left(-\frac{600}{T}\right)\exp\left(\frac{700(T_e-T)}{T_eT}\right)$	$[m^6/s]$	Ref. 34
$e + O_2 + N_2 \rightarrow O_2^- + N_2$	$1.07 \times 10^{-43}\left(\frac{300}{T_e}\right)\exp\left(-\frac{70}{T}\right)\exp\left(\frac{1500(T_e-T)}{T_eT}\right)$	$[m^6/s]$	Ref. 34
$O_2^+ + O_2 + O_2 \rightarrow O_4^+ + O_2$	$2.4 \times 10^{-42}\left(\frac{300}{T}\right)^{3.2}$	$[m^6/s]$	Ref. 34
$N_2^+ + N_2 + N_2 \rightarrow N_4^+ + N_2$	$5 \cdot 10^{-41}$	$[m^6/s]$	Ref. 34
$N_4^+ + N_2 \rightarrow N_2^+ + N_2 + N_2$	$10^{-6} \cdot 10^{[-14.6+0.0036*(T-300)]}$	$[m^3/s]$	Ref. 34
$N_4^+ + O_2 \rightarrow O_2^+ + N_2 + N_2$	2.5×10^{-16}	$[m^3/s]$	Ref. 34
$O_4^+ + O_2 \rightarrow O_2^+ + O_2 + O_2$	$3.3 \times 10^{-12}\left(\frac{300}{T}\right)^4\exp\left(-\frac{5030}{T}\right)$	$[m^3/s]$	Ref. 34
$e + N_4^+ \rightarrow N_2 + N_2$	$2 \cdot 10^{-12}\left(\frac{300}{T_e}\right)^{1/2}$	$[m^3/s]$	Ref. 34
$e + O_4^+ \rightarrow O_2 + O_2$	$1.4 \times 10^{-12}\left(\frac{300}{T_e}\right)^{1/2}$	$[m^3/s]$	Ref. 34
$e + N_2^+ \rightarrow N + N$	$2.8 \times 10^{-13}\left(\frac{300}{T_e}\right)^{1/2}$	$[m^3/s]$	Ref. 34
$e + O_2^+ \rightarrow O + O$	$2 \cdot 10^{-13}\left(\frac{300}{T_e}\right)$	$[m^3/s]$	Ref. 34
$e + NO^+ \rightarrow N + O$	$4 \cdot 10^{-13}\left(\frac{300}{T_e}\right)^{1.5}$	$[m^3/s]$	Ref. 34
$e + O + O_2 \rightarrow O_2^- + O$	$1 \cdot 10^{-43}$	$[m^6/s]$	Ref. 34
$O_2^- + O \rightarrow O_3 + e$	1.5×10^{-16}	$[m^3/s]$	Ref. 34
$O_2 + N \rightarrow NO + O$	$1.1 \times 10^{-20}\mathrm{T}\exp\left(-\frac{3150}{T}\right)$	$[m^3/s]$	Ref. 34
$O^+ + N + M \rightarrow NO^+ + M; \quad M = O_2, N_2$	$1 \cdot 10^{-41}$	$[m^6/s]$	Ref. 34
$N^+ + O_2 \rightarrow O_2^+ + N$	2.8×10^{-16}	$[m^3/s]$	Ref. 34
$N^+ + O_2 \rightarrow NO^+ + O$	2.5×10^{-16}	$[m^3/s]$	Ref. 34
$N^+ + O \rightarrow N + O^+$	$1 \cdot 10^{-18}$	$[m^3/s]$	Ref. 34
$N^+ + O_3 \rightarrow NO^+ + O_2$	$5 \cdot 10^{-16}$	$[m^3/s]$	Ref. 34
$N^+ + NO \rightarrow N + NO^+$	$8 \cdot 10^{-16}$	$[m^3/s]$	Ref. 34
$N^+ + NO \rightarrow N_2^+ + O$	$3 \cdot 10^{-18}$	$[m^3/s]$	Ref. 34
$N^+ + NO \rightarrow O^+ + N_2$	$1 \cdot 10^{-18}$	$[m^3/s]$	Ref. 34
$O^+ + N_2 \rightarrow NO^+ + N$	$3 \cdot 10^{-18}\exp(-0.00311 \cdot \mathrm{T})$	$[m^3/s]$	Ref. 34
$N_2^+ + O_2 \rightarrow O_2^+ + N_2$	$6 \cdot 10^{-17}\left(\frac{300}{T}\right)^{1/2}$	$[m^3/s]$	Ref. 34
$N_2^+ + O \rightarrow NO^+ + N$	$1.3 \times 10^{-10}\left(\frac{300}{T}\right)^{1/2}$	$[m^3/s]$	Ref. 34
$N_2^+ + O \rightarrow O^+ + N_2$	$1 \cdot 10^{-17}\left(\frac{300}{T}\right)^{0.2}$	$[m^3/s]$	Ref. 34
$N_2^+ + O_3 \rightarrow O_2^+ + O + N$	$1 \cdot 10^{-16}$	$[m^3/s]$	Ref. 34
$N_2^+ + NO \rightarrow NO^+ + N_2$	3.3×10^{-16}	$[m^3/s]$	Ref. 34
$O_2^+ + N_2 \rightarrow NO^+ + NO$	$1 \cdot 10^{-23}$	$[m^3/s]$	Ref. 34
$O_2^+ + N \rightarrow NO^+ + O$	1.2×10^{-16}	$[m^3/s]$	Ref. 34
$O_2^+ + NO \rightarrow NO^+ + O_2$	4.4×10^{-16}	$[m^3/s]$	Ref. 34
$N_4^+ + O \rightarrow O^+ + N_2 + N_2$	2.5×10^{-16}	$[m^3/s]$	Ref. 34
$N_4^+ + N \rightarrow N^+ + N_2 + N_2$	$1 \cdot 10^{-17}$	$[m^3/s]$	Ref. 34
$N_4^+ + NO \rightarrow NO^+ + N_2 + N_2$	$4 \cdot 10^{-16}$	$[m^3/s]$	Ref. 34
$O_4^+ + O \rightarrow O_2^+ + O_3$	$3 \cdot 10^{-16}$	$[m^3/s]$	Ref. 34
$O_4^+ + NO \rightarrow NO^+ + O_2 + O_2$	$1 \cdot 10^{-16}$	$[m^3/s]$	Ref. 34
$O_2^- + O_2 \rightarrow e + O_2 + O_2$	$8.6 \times 10^{-16}\exp\left(-\frac{6030}{T}\right)\left[1-\exp\left(-\frac{1570}{T}\right)\right]$	$[m^3/s]$	Ref. 34
$\hbar\omega_L + O_2^-(^4\Sigma_g^-) \rightarrow e + O_2(^3\Sigma_g^-); \quad \sigma_{ph}(\hbar\omega_L)$			Ref. 27
$O_2^- + O_2^+ \rightarrow O_2 + O_2$ $O_2^- + N_2^+ \rightarrow O_2 + N_2$	$\begin{cases} 2.2 \times 10^{-12}(\rho/\rho_0)^{1.5}, & \rho \le \rho_0 \\ 2.2 \times 10^{-12}(\rho_0/\rho)^{1.2}, & \rho > \rho_0 \end{cases}$ ρ_0 is the air density at STP	$[m^3/s]$	Ref. 24

TABLE I. (*Continued*)

$e + O + O_2 \rightarrow O^- + O_2$	1.10^{-43}	$[m^3/s]$	Ref. 34
$e + O_3 \rightarrow O + O_2^-$	1.10^{-15}	$[m^3/s]$	Ref. 34
$e + O_3 \rightarrow O^- + O_2$	1.10^{-17}	$[m^3/s]$	Ref. 34
$O^- + O \rightarrow O_2 + e$	5.10^{-16}	$[m^3/s]$	Ref. 34
$O^- + N \rightarrow NO + e$	2.6×10^{-16}	$[m^3/s]$	Ref. 34
$O^- + O_2 \rightarrow O_3 + e$	5.10^{-21}	$[m^3/s]$	Ref. 34

is the Joule heat, $\lambda_e = 5kn_eD_e/2$ is the electron heat conductivity, v_{ex} is the rate of electronic level excitation, and I^* is the relevant effective excitation energy.

The electronic and vibrational excitation rates are calculated using the model of Ref. 29,

$$v_{ex}(T_e) = 5.53 \times 10^6 (N/N_0) T_e^2 (1812.23 + T_e^{-15}) \times \exp(-1.7835/T_e^2), \quad (24)$$

$$v_{ev}(T_e) \approx [8.917 \cdot 10^{10} T_e^{-3} (9.93 + T_e^5) \exp(-2.36/T_e^3) - v_{ex}(T_e) I^*]/\hbar\omega_0, \quad (25)$$

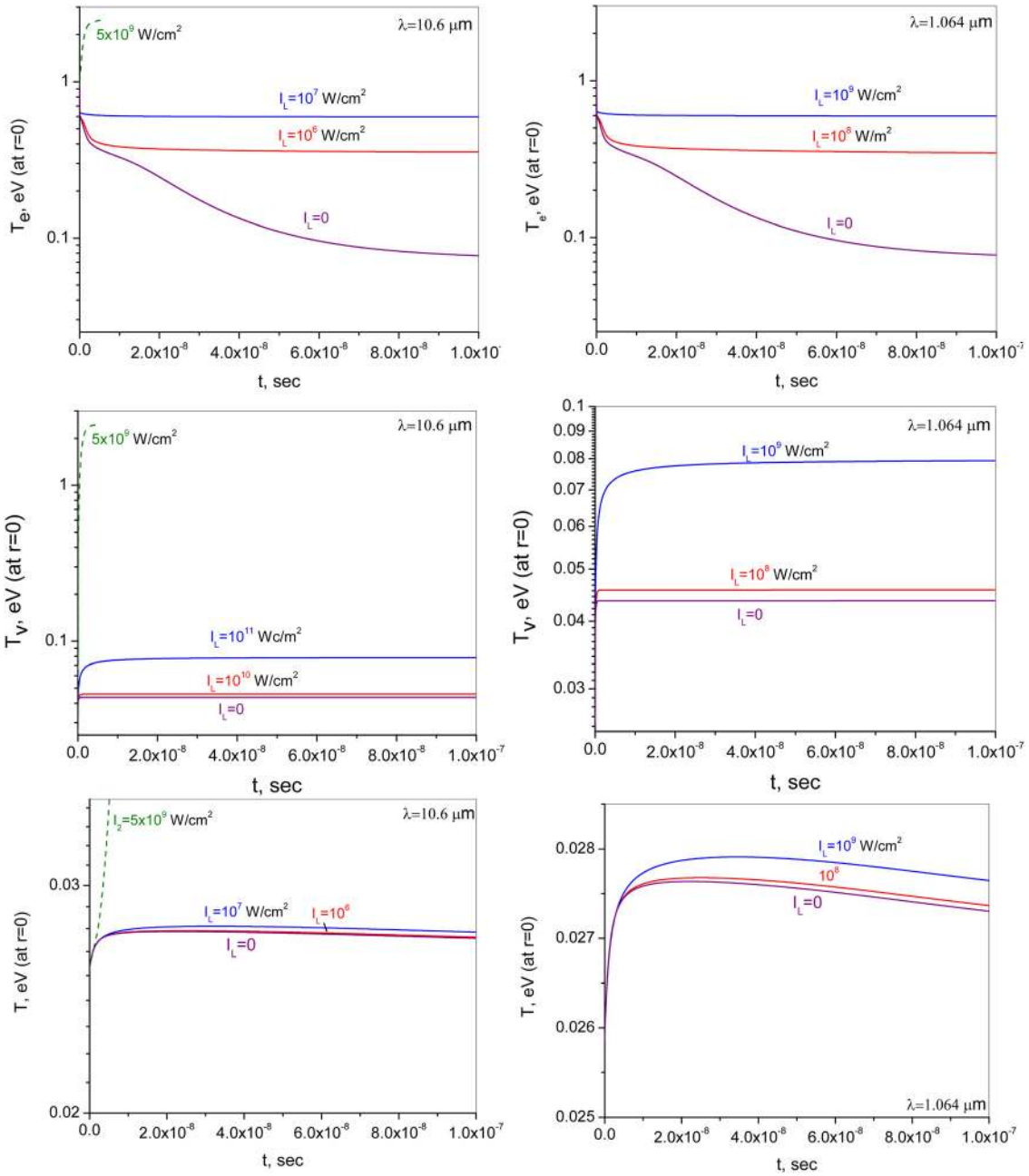

FIG. 1. (Color online) Time dependences of the electron (upper), vibrational (middle), and translational (lower) temperatures in the wake of a laser-induced filament in the atmosphere in the absence ($I_2 = 0$) and in the presence of laser radiation with (left column) $\lambda_L = 10.6$ μm and $I_L = 10^6$ W/cm^2, 10^7 W/cm^2 and (right column) $\lambda_L = 1.06$ μm, $I_L = 10^8$ W/cm^2 and 10^9 W/cm^2. In the left three figures, the breakdown development at $I_L = 5 \times 10^9$ W/cm^2 is shown.

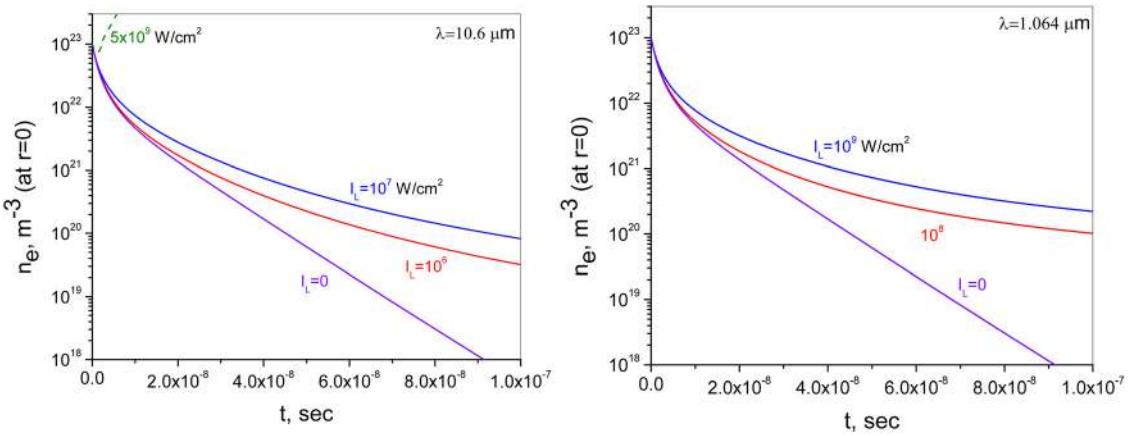

FIG. 2. (Color online) Time dependences of the electron density n_e on the axis in the wake of a laser-induced filament in the atmosphere in the absence or presence of laser radiation with a wavelength $\lambda_L = 10.6$ μm (left) and $\lambda_L = 1.06$ μm (right). In the left column figures, the breakdown development at $I_L = 5\times10^9$ W/cm^2 is shown.

where the electron temperatures are expressed in eV, N_0 is the gas density at a pressure of 1 atm and a temperature of 300 K, and I^* is the effective excitation energy, which is taken equal to 10 eV.[29]

The other processes included in the model along with their rate constants are listed in Table I. Our model neglects two-body dissociative attachment processes, such as $e + O_2 + \delta W \rightarrow O^- + O$ ($\delta W \approx 3.6$ eV), since the electron energies acquired within the considered range of laser intensities are well below the activation energy of such processes.

RESULTS AND DISCUSSION

The above-described model is applied to simulate plasma dynamics in an individual filament created by a femtosecond laser pulse with the above-specified parameters. We assume that the plasma produced in the wake of a laser filament is irradiated by an additional laser pulse, which is turned on at the instant of time $t = 0$ with its intensity I_L remaining constant over a time interval of hundreds of nanoseconds. This additional laser beam is assumed to be loosely focused in such a way as to provide constant field intensity over the filament area. We examine plasma dynamics in the presence of radiation delivered by one of the two widely used laser sources—a neodymium laser ($\lambda_L = 2\pi c/\omega_L = 1.06$ μm) and a CO_2 laser ($\lambda_L = 10.6$ μm). The laser intensity provided by both lasers is assumed to be too low to induce any noticeable multiphoton or tunneling ionization of the medium. In this regime, an additional laser pulse decelerates plasma decay primarily through the suppression of three-body electron attachment and dissociative recombination processes. In addition to these two mechanisms, the photons of 1.06-μm radiation are energetic enough ($\hbar\omega_L \approx 1.17$ eV) to slow down the plasma decay through the photodetachment of electrons from neutral species (the activation energy is about 0.5 eV). In the case of a CO_2 laser, no electron photodetachment can be induced because of the low energy of laser photons ($\hbar\omega_L \approx 0.12$ eV).

Application of a low-intensity infrared laser pulse can radically modify the plasma dynamics in the wake of a laser-induced filament (Figs. 2–5). With the intensity of Nd-laser radiation taken two orders of magnitude higher than the intensity of CO_2-laser pulses, to compensate for the $\propto \omega_L^{-2}$ scaling of plasma-heating efficiency (see Eq. (23)), Nd- and CO_2-laser pulses give rise to similar tendencies in plasma

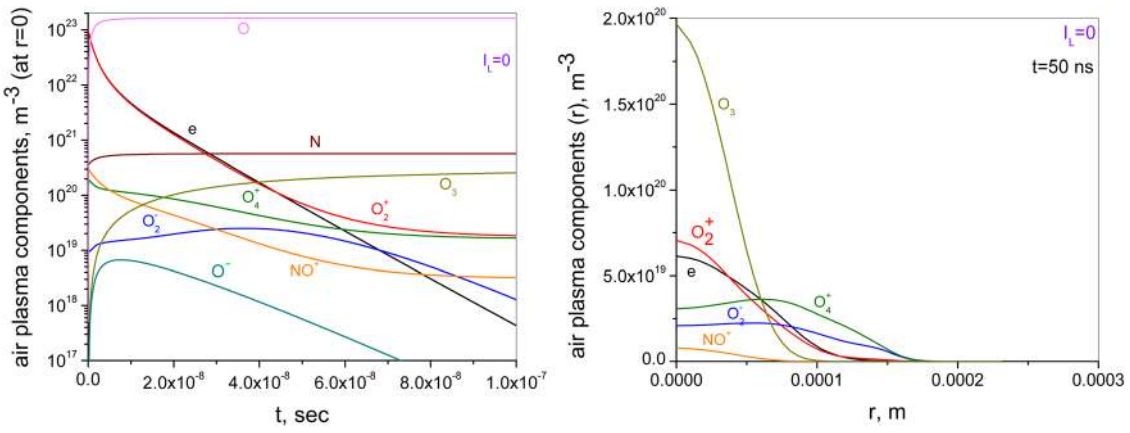

FIG. 3. (Color online) Time-evolution of air plasma components on a filament axis (left) and a radial distribution at t = 50 ns (right) in the absence of laser radiation.

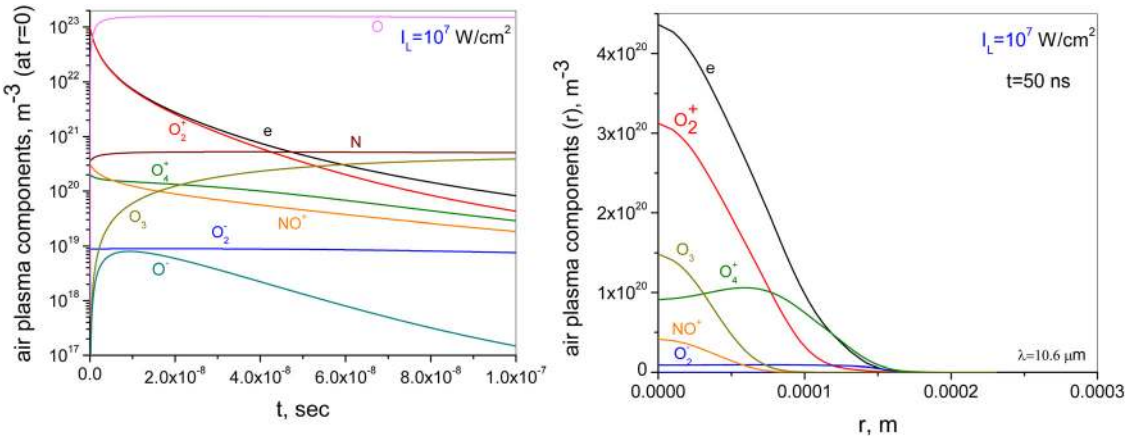

FIG. 4. (Color online) Time-evolution of air plasma components on a filament axis (left) and a radial distribution at t = 50 ns (right) in the presence of IR CO_2 laser radiation with $\lambda_L = 10.6$ μm and $I_L = 10^7$ W/cm^2.

dynamics. These laser pulses heat plasma electrons, sustaining a large gap between the electron and vibrational temperatures on the time scale of hundreds of nanoseconds, with higher intensities I_L translating into wider temperature gaps δT at a given instant of time (see Fig. 1). An increase in the electron temperature suppresses electron attachment to oxygen molecules and decelerates dissociative recombination, with the relevant rate constants scaling as $\beta \propto T_e^{-\xi}$, where $0.5 \leq \xi < 1.5$ for recombination rates for different molecular ions (see Table I). As a result, the electron density is high over an extended time interval at $t = 100$ ns and $n_e \approx 8.5 \times 10^{19}$ m^{-3} for CO_2-laser pulses with $I_L = 10^7$ W/cm^2 (Fig. 3, left) and $n_e \approx 2.3 \times 10^{20}$ m^{-3} for Nd-laser pulses with $I_L = 10^9$ W/cm^2 (Fig. 4, left). The corresponding plasma frequencies $\omega_p = \sqrt{e^2 n_e/\varepsilon_0 m}$ are 5.2×10^{11} and 8.5×10^{11} 1/s. It means, in accordance with Refs. 15 and 16], that an array of such filaments can be maintained to guide microwave radiation at $f = 30$ GHz (angular frequency $\omega = 2\pi f \approx 1.9 \times 10^{11}$ rad/s) at $t > 100$ ns.

At elevated intensities of the second ns laser pulse (still below breakdown of surrounding air), intense ionization and Joule heating in the initial filament can increase the conditions up to those typical for a high conductive arc discharge. The initial phase of this process is shown in Figs. 1 and 2 for the case of IR CO_2-laser radiation at λ_L=10.6 μm and $I_L = 5 \times 10^9$ W/cm^2 (the model considered in this paper is not applicable to the description of transition to the arc-kind plasma regime, because it deals only with electron impact ionization, but not thermal ionization, which becomes dominant at a high gas temperatures). As a result, a highly conductive long channel is generated, which may be used in lightning-protection systems. It was shown that the rate of arc-like channel decay may be controlled with additional residual heating by a series of defocused ns-laser pulses with repetition rate ~1–10 kHz. The physics of sustaining conductivity in a channel is similar to what is studied theoretically in Refs. 30 and 31 and experimentally (for a small-scale laboratory pulsed arc).[32]

PLASMA-FILAMENT–HEATING-PULSE INTERACTION LENGTH

The radial distribution of the electron density $n_e(r)$ in the filament plasma across the laser beam translates into a transverse profile of refractive index, giving rise to a negative lens. This lens defocuses the heating laser pulse, limiting the effective length of interaction of this pulse with the

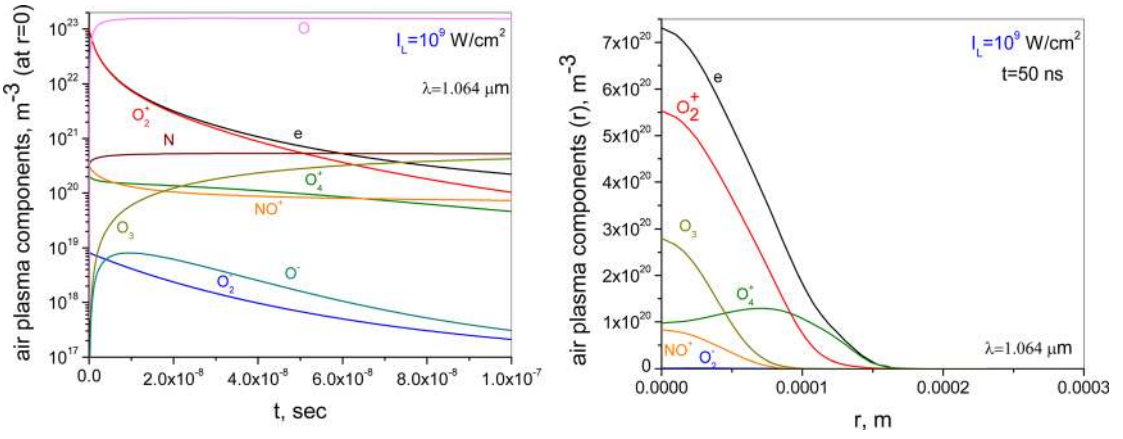

FIG. 5. (Color online) Time-evolution of air plasma components on a filament axis (left) and a radial distribution at t = 50 ns (right) in the presence of Nd-laser laser radiation with $\lambda_L = 1.064$ μm and and $I_L = 10^9$ W/cm^2.

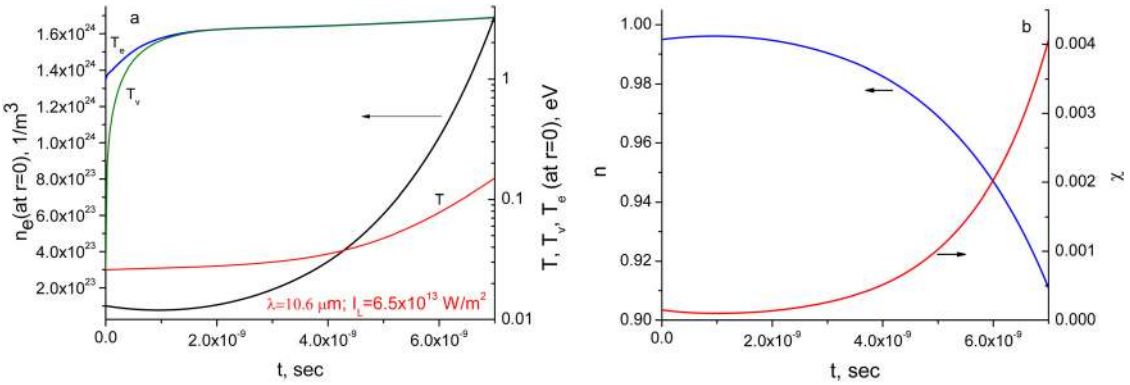

FIG. 6. (Color online) Time evolution of (a) the electron density (n_e) and the electron (T_e), vibrational (T_u), and gas (T_e) temperatures and (b) refractive index (n) and absorption coefficient χ on the axis of the filament in the presence of a heating CO_2 laser pulse with $\lambda_L = 10.6$ μm and $I_L = 6.5.10^9$ W/cm^2.

plasma produced by a filament, thus preventing a uniform heating of the plasma by the nanosecond laser pulse. To identify the regimes where this effect can be minimized, we calculate the refractive index (n) and absorption coefficient (χ) of the plasma medium as[24]

$$n = \sqrt{\frac{\varepsilon + \sqrt{\varepsilon^2 + (\sigma/\varepsilon_0\omega_L)^2}}{2}} \le 1,$$
$$\chi = \sqrt{\frac{-\varepsilon + \sqrt{\varepsilon^2 + (\sigma/\varepsilon_0\omega_L)^2}}{2}}, \qquad (31)$$

where $\varepsilon = 1 - \frac{\omega_p^2}{\omega_L^2 + (\nu_m + \nu_c)^2}$, $\sigma = \frac{e^2 n_e (\nu_m + \nu_c)}{m[\omega_L^2 + (\nu_m + \nu_c)^2]}$ are the dielectric function and conductivity of the plasma.

In Fig. 6(a), the early phase of breakdown development for the case of infrared CO_2-laser ($\lambda = 10.6$ μm) with intensity 6.5×10^9 W/cm^2 is shown. The corresponding evolution of the index of refraction and absorption coefficient on the filament axis are shown in Fig. 6(b).

The heating-pulse−postfilament-plasma interaction efficiency is almost insensitive to the focusing of the heating laser beam, but is primarily controlled by the efficiency of coupling of this beam into the postfilament plasma. Large gradients of the electron density in the postfilament plasma would strongly defocus the heating laser beam and should therefore be avoided. To illustrate this argument, we plot in Figs. 7(a)–7(c) the radial profiles of the electron density and the corresponding index of refraction and absorption coefficient. The radial profiles of the refractive index $n(r)$ found from these simulations are used to analyze the ray trajectories of the heating pulse by using the eikonal-approximation equation $z(r) = \bar{\beta} \int_0^r \left[n^2(r) - \bar{\beta}^2\right]^{-1/2} dr$, where the z-axis is chosen along the plasma column and $\bar{\beta} = n(r)dz/ds$ is the ray invariant, s being the path measured along the beam trajectory.[33] For a plasma column with a radius of 50 μm and a refractive index change $\Delta n \approx 5 \times 10^{-2}$ (Fig. 7(b)), the resulting negative lens will give rise to an additional divergence of a laser beam $\theta_{pl} \sim 1$ within a plasma length of only $\sim$1 mm. In this regime, strong defocusing of the heating laser beam by the transverse profile of the electron density will prevent the efficient coupling of the laser beam into the plasma column in the wake of the filament, rendering a uniform heating of this column impossible. For weaker electron-density gradients, e.g., those corresponding to an on-axis electron density of $\sim 10^{16}$ cm^{-3}, the plasma-induced change in the refractive index in the postfilament plasma is $\Delta n \approx 5 \times 10^{-5}$. A beam divergence $\theta_{pl} = 1$ is then achieved within a plasma length of 1 m, enabling a uniform heating of extended regions of ionized gas in the wake of a filament and sustain guiding of microwave radiation.[15,16]

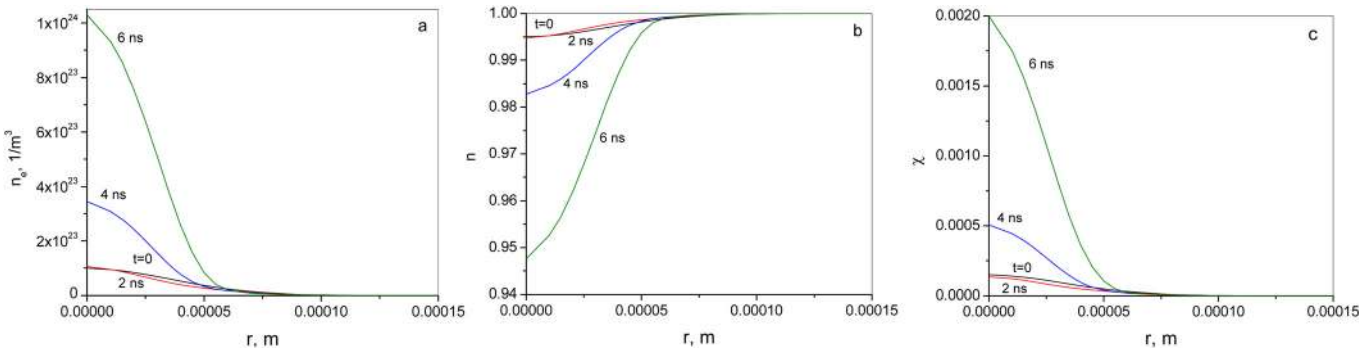

FIG. 7. (Color online) The radial profiles of the electron density (a), refractive index (b), and absorption coefficient (c) in the presence of a heating CO_2 laser pulse with $\lambda_L = 10.6$ μm and $I_L = 6.5.10^9$ W/cm^2.

CONCLUSION

We have presented a detailed model of plasma dynamics in the wake of a filament induced in the atmosphere by an ultrashort laser pulse. Analysis performed with the use of this model helps quantify the limitations on the lifetime of microwave plasma waveguides induced in the atmosphere through the filamentation of high-intensity ultrashort laser pulses. We have demonstrated that, near- and mid-infrared laser pulses can tailor the plasma decay in the wake of a filament, efficiently suppressing, through electron temperature increase, the attachment of electrons to neutral species and dissociative recombination, thus substantially increasing the plasma-guide lifetime and facilitating long-distance transmission of microwaves. Postfilament plasma lifetimes of tens to hundreds of nanoseconds demonstrated in this paper suggest that the laser pulses with pulse widths ranging from hundreds of nanoseconds to several microseconds would provide an ideal tool to sustain the plasmas and tailor plasma parameters in the wake of a laser-induced filament. Microsecond pulses of 10.6-μm radiation within the above-specified range of field intensities can be delivered by CO_2 lasers, while appropriate laser pulses with a wavelength around 1.06 μm can be generated by neodymium-doped lasers. The available neodymium-based and CO_2 lasers enable the generation of 1.06- and 10.6-μm pulses with the required intensities and pulse widths at kilohertz repetition rates. Laser pulses with higher intensities can give rise to efficient ionization and heating of the postfilament plasma, eventually inducing a highly conductive arc discharge. Highly conductive long plasma channels generated as a result of this process would offer promising solutions for lightning protection. However, the plasma-filament−heating-pulse longitudinally uniform interaction length is limited due to the self-defocusing of the heating beam. This effect becomes important when subsequent heating laser pulse is focused to values close to breakdown and it depends on the laser wavelength.

ACKNOWLEDGMENTS

We are grateful to Dr. Phillip Sprangle and Dr. Daniel Gordon from NRL for helpful discussions. The work by MNS and RBM was supported by the Science Addressing Asymmetric Explosive Threats (SAAET) Program of the U.S. Office of Naval Research. AMZ acknowledges a partial support of his research by the Seventh European Framework Programme under project No. #244068 (CROSS TRAP).

[1]E. H. Piepmeier and H. V. Malmstadt, Anal. Chem. **41**, 700 (1969).
[2]R. H. Scott and A. Strasheim, Spectrochim. Acta, Part B **25**, 311 (1970).
[3]S. M. Gladkov, A. M. Zheltikov, N. I. Koroteev, M. V. Rychev, and A. B. Fedotov, Sov. J. Quantum Electron. **19**, 923 (1989).
[4]Z. Henis, G. Milikh, K. Papadopoulos, and A. Zigler, J. Appl. Phys. **103**, 103111 (2008).
[5]B. Zhou, S. Akturk, B. Prade, Y.-B. André, A. Houard, Y. Liu, M. Franco, C. D'Amico, E. Salmon, Z.-Q. Hao, N. Lascoux, and A. Mysyrowicz, Opt. Express **17**, 11450 (2009).
[6]M. N. Shneider, Z. Zhang, and R. B. Miles, J. Appl. Phys. **104**, 023302 (2008).
[7]T. B. Petrova, H. D. Ladouceur, and A. P. Baronavski, Phys. Plasmas **15**, 053501 (2008).
[8]D. F. Gordon, A. Ting, R. F. Hubbard, E. Briscoe, C. Manka, S. P. Slinker, A. P. Baronavski, H. D. Ladouceur, P. W. Grounds, and P. G. Girardi, Phys. Plasmas **10**, 4530 (2003).
[9]R. B. Miles, Z. Zhang, S. H. Zaidi, and M. N. Shneider, AIAA J. **54**(3), 513 (2007).
[10]P. R. Hemmer, R. B. Miles, P. Polynkin, T. Siebert, A. V. Sokolov, P. Sprangle, and M. O. Scully, in Proc. Natl. Acad. Sci. U S A. **108**(8) 3130 (2011).
[11]J. D. Dale, P. R Smy, and R. M. Clements, "Laser ignited internal combustion engine—An experimental study," SAE Paper No. 780329, 1979.
[12]A. Stakhiv, R. Gilber, H. Kopecek, A. M. Zheltikov, and E. Wintner, Laser Phys. **14**, 738 (2004).
[13]J. B. Michael, A. Dogariu, M. N. Shneider, and R. B. Miles, J. Appl. Phys. **108**, 093308 (2010).
[14]A. M. Zheltikov, M. N. Shneider, and R. B. Miles, Appl. Phys. B **83**, 149 (2006).
[15]R. R. Musin, M. N. Shneider, A. M. Zheltikov, and R. B. Miles, Appl. Opt. **46**, 5593 (2007).
[16]M. N. Shneider, A. M. Zheltikov, and R. B. Miles, J. Appl. Phys. **108**, 033113 (2010).
[17]M. Châteauneuf, S. Payeur, J. Dubois, and J.-C. Kieffer, Appl. Phys. Lett. **92**, 091104 (2008).
[18]V. D. Zvorykin, A. O. Levchenko, N. N. Ustinovskii, and I. V. Smetanin, JETP Lett. **91**, 226 (2010).
[19]K. Mishima, K. Nagaya, M. Hayashi, and S. H. Lin, J. Chem. Phys. **122**, 104312 (2005).
[20]L. V. Keldysh, Zh. Eksp. Teor. Fiz. **47**, 1945 (1964) [Sov. Phys. JETP **20**, 1307 (1964)].
[21]P. Sprangle, J. R. Penano, and B. Hafizi, Phys. Rev. E **66**, 046418 (2002).
[22]L. Bergé, S. Skupin, R. Nuter, J. Kasparian, and J.-P. Wolf, Rep. Prog. Phys. **70**, 1633 (2007).
[23]A. Couairon and A. Mysyrowicz, Phys. Rep. **441**, 47 (2007).
[24]Y. P. Raizer, *Gas Discharge Physics* (Springer, New York, 1997).
[25]A. V. Gurevich, N. D. Borisov, and G. M. Milikh, *Physics of Microwave Discharges Artificially Ionized Regions of the Atmosphere* (Gordon and Breach Science, Amsterdam, 1997).
[26]W. Ali, "The electron avalanche ionization of air and a simple air chemistry model," NRL Memorandum Report 4794, April 1982.
[27]D. S. Bursh, S. J. Smith, and L. M. Branscomb, Phys. Rev. **112**, 171 (1958).
[28]D. Khmara, Y. Kolesnichenko, and D. Knight, "Modeling of microwave filament origination," in *Proceedings of the 44th AIAA Aerospace Sciences Meeting and Exhibit, Reno, Nevada, 9–12 January 2006*, AIAA Paper 2006-794.
[29]A. V. Ivanovskii, Tech. Phys. **45**, 710 (2000).
[30]N. L. Aleksandrov, E. M. Bazelyan, and M. N. Shneider, Plasma Phys. Rep. **26**, 893 (2000).
[31]M. N. Shneider, Phys. Plasmas **13**, 073501 (2006).
[32]S. V. Leonov, Y. I. Isaenkov, and M. N. Shneider, Phys. Plasmas **14**, 123504 (2007).
[33]M. Born and E. Wolf, *Principles of Optics: Electromagnetic Theory of Propagation, Interference and Diffraction of Light*, 7th ed. (Cambridge University Press, New York, 1999).
[34]I. A. Kossyi, A. Y. Kostinsky, A. A. Matveyev, and V. P. Silakov, Plasma Sources Sci. Technol. **1**, 207 (1992).